

Vanadium dioxide nanobeams: probing sub-domain properties of strongly correlated materials using nanostructures

Jiang Wei†, Zenghui Wang†, Wei Chen†, and David H. Cobden†

† Department of Physics, University of Washington, Seattle WA 98195-1560

It is widely recognized that when the size of a nanoscale sample is comparable with electronic length scales it can demonstrate very different behavior from the bulk material. However, in many materials there is another important length scale – that of the domain structure, which exists as a result of long range forces (magnetic, electric or elastic) competing with short range ordering forces. Domain structure causes the bulk properties to differ from those on the sub-domain level; moreover, near first-order phase transitions it leads to transition broadening, hysteresis, and sample degradation. Another reason therefore to study nanoscale crystals is that they enable investigations of the domain-free homogeneous material. We demonstrate this by working with nanobeams of vanadium dioxide, thereby discovering or clarifying multiple aspects of its famous metal-insulator transition¹⁻³ at 67 °C. Amongst them are that the transition to the metal occurs at a constant value of the resistivity of the insulating phase; the transition always proceeds via an intermediate insulating structure which has three times higher resistivity; large supercooling of the homogeneous metallic phase is possible; and the activation energy in the insulating phase is consistent with the optical gap, in contrast with earlier reports on bulk samples. The nanobeams also enable new classes of experiments, including investigating a single metal-insulator interphase wall, employing nanomechanical effects to determine the equilibrium transition temperature, and investigating the dynamics of a phase transition in quasi-one-dimensional geometry.

At temperatures above $T_c \approx 67$ °C, bulk VO₂ is a poor metal, while below T_c it is a semiconductor with an optical gap⁴ $E_g = 0.6$ eV. The transition to the metal can be induced very rapidly and has recently been studied intensively by ultrafast techniques.⁵⁻¹¹ The lattice in the metallic phase has the rutile (R) structure, with the vanadium ions arranged in periodic chains parallel to the c -axis. In the lower symmetry insulating phase these are distorted into dimerized zig-zag chains, resulting in a monoclinic structure known as M1. An additional monoclinic insulating phase^{12,13} known as M2, in which only half the chains are dimerized, can be stabilized below T_c by chromium doping,^{14,15} reduced oxygen content,¹⁶ or uniaxial compression perpendicular to the rutile c -axis,¹⁷ with a transition between M2 and M1 then occurring at lower temperature.

Many factors indicate that the transition involves strong electron-electron correlations. These include the anomalously low conductivity and other properties of the metal;¹⁸⁻²⁰ the fact that band structure calculations fail to yield the insulator band gap;^{3,21} the fact that M2 is insulating in spite of its undimerized chains;²² and the dependence on optical excitation energy which indicates sensitivity to excited carrier density.^{9,10,23} On the other hand, other factors suggest that some lattice reconfiguration is necessary before the metallic phase can appear. For example, the metallic conductivity takes ~ 75 fs to develop after optical excitation of an M1 crystal,^{8,11} which is slow for a purely electronic process but comparable with an inverse optic phonon frequency.

However, the precise nature of the transition remains unclear half a century after its discovery¹, and promising applications in bolometry and optical switching are still unrealized. The blame for this falls largely on the domain structure, which leads to irreproducibility between samples (properties such as the resistivity are very sensitive to the exact arrangement of

domains), broadening and hysteresis of characteristics, and nonuniform stresses producing cracking¹⁸. All these problems are absent in our nanobeam devices.

The nanobeams were grown directly on oxidized Si wafers by a physical vapor transport technique based on that introduced by Park's group:^{24,25} the substrate was placed in 20 mbar Ar carrier gas downstream from a granular VO₂ source in a tube furnace at 1000 °C for about 30 minutes. Each nanobeam is a single crystal elongated along the rutile *c*-axis. The length can be hundreds of microns, and the cross-section is roughly rectangular with width W down to 50 nm and thickness H down to 15 nm. As reported by Wu *et al.*,²⁵ on warming, quasiperiodic thin stripes of darker metallic phase can be seen to appear around 60 °C in an optical microscope (Fig. 1a). The stripes then widen and the lighter insulating phase entirely disappears by around 105 °C. This behaviour results from strain caused by the firm attachment to the SiO₂ substrate. A fully insulating nanobeam is under compressive axial strain, while a fully metallic one, having a smaller equilibrium *c*-axis lattice constant, is under tension. Alternation of metallic and insulating domains reduces the average strain, at the cost of creating interphase walls. Wu *et al.* also found that if the nanobeams are released from the substrate, completely relieving the strain, the transition becomes sudden with no stable domain pattern formation.

Here, instead of eliminating the axial strain, we exploit it. Using electron-beam or optical lithography we pattern a series of electron-beam evaporated metal contacts (10 nm vanadium under 400 nm gold) onto a nanobeam, and then immerse in buffered oxide etch to remove the 1 μm-thick SiO₂ where it is not covered by metal and thereby to suspend the nanobeam sections between the contacts. The behaviour of the resulting devices, under repeated cycling in air between 120 °C and room temperature, $T_{\text{room}} \approx 30$ °C, can be reproducible over months, although it is modified significantly by passing large currents or storage in vacuum. At T_{room} , shorter sections are straight while longer ones are buckled (Fig. 1b). This is consistent with the behaviour of clamped beams, in which Euler buckling occurs when the compressive axial stress p exceeds a critical value p_b that is smaller for longer beams. Firm adhesion to the substrate under the contacts provides the clamping. After buckling the compressive axial strain, $\eta = p/E$, where E is the Young's modulus, is mostly relieved, so p is much smaller and the nanobeam adopts approximately its natural length, L_0 . By taking L_0 to be the length measured along the curved profile of a buckled section measured in an atomic force microscope, and calling the contact separation L , we find that the substrate-induced strain in most straight nanobeams at T_{room} is $\eta_0 = (L_0 - L)/L = 0.4 \pm 0.1$ %.

Seen in an optical microscope, between about 68 and 105 °C every segment of each nanobeam is unbuckled and consists of one metallic and one insulating region coexisting and separated by a single interphase wall (see Fig. 1c). As T increases, the fraction x of insulating phase, plotted in Fig. 1d, decreases steadily until at a temperature T_m of about 105 °C the nanobeam becomes fully metallic. This can be understood by noting that given fixed L , once the nanobeam begins to convert from insulator to metal its equilibrium length L_0 decreases and so therefore do both η and p . At a particular T the fraction x of insulator adjusts so that p is appropriate for the two phases to coexist, ie, to lie on the phase boundary line between insulator and metal in the (p, T) -plane, as sketched in Fig. 1e. The stress p should be zero at $T = T_c$ and negative (tensile) at higher T , explaining why all nanobeams become straight above about 68 °C.

The nanobeam thus provides a one-dimensional (1D) analog of the 3D situation of a sealed vessel filled with water near 0 °C: there too the low- T phase (ice) has higher volume and lower symmetry than the high- T phase (liquid water), and the fraction x of ice decreases as T increases

in a corresponding way. Note that in the coexistence regime the nanobeam should have zero axial stiffness, just as the ice-water mixture has diverging compressibility.

Taking the Young's modulus E to be the same for both phases,²⁶ the strain $\eta(T)$ is uniform along the nanobeam and the equilibrium phase boundary $p(T)$ is determined by

$$p(T)/E = \eta(T) = \alpha(x - x_c) + K(T - T_c). \quad (1)$$

The first term on the right represents interconversion between the phases, where α is the fractional increase in rutile c-axis length going from metal to insulator and x_c is the insulating fraction at $T = T_c$. x_c depends on the built-in strain relative to the substrate, which could depend on growth conditions. The second term represents differential thermal expansion of the VO₂ relative to the Si substrate. It is an order of magnitude smaller than the first term, the value of K being $\sim +2.0 \times 10^{-5} \text{ }^\circ\text{C}^{-1}$, and we take K to be independent of T and the same for both phases since there is no clear indication otherwise in the literature.^{25,27,28}

Eq. (1) implies that x should have the same variation with T for every nanobeam, to within an offset x_c . The data in Fig. 1d agree well with this prediction. In addition we observe that $x(T)$ is nearly a straight line, with $dx/dT = -(1.10 \pm 0.05) \times 10^{-2} \text{ }^\circ\text{C}^{-1}$. This implies that the phase boundary line is nearly straight, so we can write

$$p(T)/E = \beta(T - T_c), \quad (2)$$

where $\beta = \alpha dx/dT + K$ is a constant. According to Eq. (2), p will become positive when a nanobeam in coexistence is cooled below T_c , and upon further cooling we expect the nanobeam to buckle at a temperature T_b such that $p(T_b) = p_b$. Using the Euler expression for the buckling pressure of a doubly clamped beam, $p_b = (\pi^2 E/3)H^2/L^2$, we then have

$$\beta(T_c - T_b) = (\pi^2/3)H^2/L^2.$$

This predicts that a plot of T_b vs $1/L^2$ will yield a straight line with y -intercept $T_c = \lim_{L \rightarrow \infty}(T_b)$. In Fig. 1f we make such a plot for a series of sections of a nanobeam of thickness $H = 180 \pm 5$ nm. The data are indeed well fitted by the straight line shown, with slope $\partial T_b / \partial (L^{-2}) = -820 \pm 20 \text{ }^\circ\text{C } \mu\text{m}^2$ and y -intercept $T_c = 65.7 \pm 0.2 \text{ }^\circ\text{C}$. We note that this represents a completely new way of measuring T_c that is independent of hysteresis at the transition.

From the slope we obtain $\beta = (\pi^2 H^2/3)/[\partial T_b / \partial (L^{-2})] = (-13 \pm 1) \times 10^{-5} \text{ }^\circ\text{C}^{-1}$. Knowing β , and estimating²⁶ $E \approx 140$ GPa, we can quantify the stress in the nanobeam: the phase boundary slope is $\beta E \approx -18$ MPa $^\circ\text{C}^{-1}$, and the largest tension, which is reached at $T = T_m \approx 110 \text{ }^\circ\text{C}$, is given by $p_m = \beta E(T_m - T_c) \approx -0.7$ GPa. For $T > T_m$ the nanobeam is fully metallic and thermal expansion causes the tension to decrease again, at a rate $\partial p / \partial T = KE \approx +2.5$ MPa $^\circ\text{C}^{-1}$ (as indicated in Fig. 1e). Also, using this value for β in the expression after Eq. (2) we find $\alpha = (\beta - K)/(dx/dT) = 1.36 \pm 0.15 \%$.

Thanks to the high degree of reproducibility and control possible using nanobeams, measurements of the two-terminal electrical resistance R in the coexistence regime give a number of new insights into the MIT in VO₂. We begin by discussing the characteristics of four nominally equal sections (A-D) of a single nanobeam, shown in Fig. 2a. Each comprises smooth R vs T curves punctuated by sudden jumps. On warming from T_{room} , R initially decreases in a semiconducting manner. It drops sharply at a temperature $T_n \sim 65\text{--}68 \text{ }^\circ\text{C}$ when a metallic domain appears and the nanobeam becomes straight. Subsequently, in the coexistence regime, R decreases steadily to a much smaller value at $T_m \sim 105 \text{ }^\circ\text{C}$ at which the insulating domain

disappears. The coexistence curve is reproducible on sweeping up and down at 6 °C/min, as long as T is kept below T_m . On the other hand, on cooling from above T_m each section remains metallic down to a lower temperature T_s at which an insulating domain suddenly appears and R jumps up to the coexistence curve. T_s varies greatly between sections, from 78 °C (section A) to 55 °C (section D). During further cooling, R increases smoothly until the nanobeam buckles at $T_b = 57.5$ °C. Below that, the temperature T_i at which R returns to the insulating curve also varies, as several conformations are possible after the nanobeam initially buckles downwards and collides with the substrate. When sweeping at 6 °C/min, T_s and T_n vary within a range of 2-5 °C between sweeps, while T_b and T_m are reproducible to within the measurement accuracy of about 0.1 °C.

Our first conclusion is that the homogeneous metallic phase can be supercooled to a temperature T_s which is as much as 50 °C below the phase boundary. This is represented by the green lines on the phase diagram in Fig. 2b. So much supercooling in the absence of domain structure indicates high crystal uniformity. The variation of T_s between nanobeams suggests variations in the availability of imperfections at which the insulating phase can nucleate. We note that this system offers opportunities to investigate the kinetics of a first-order phase transition in a quasi-1D geometry, for example by studying the process of insulator nucleation (at T_s) in thin nanobeams or the details of the disappearance of the insulating domain at T_m (see inset to Fig. 2a).

In Fig. 3 we plot the resistivities ρ_i and ρ_m obtained for a number of nanobeams in their fully insulating and fully metallic states simply using the relation $\rho = RA/L$, where $A = WH$. The additional measurements shown here, labeled ρ_i^{M2} and ρ_i^c , will be explained below. Studies of the dependence on L showed that contact resistance was negligible. The T dependence of ρ_i gives the same activation energy of 0.30 ± 0.01 eV for all nanobeams. Interestingly, this corresponds to the carrier density in an intrinsic semiconductor with a gap of $E_g = 0.60$ eV, which is precisely the established optical gap⁴ of VO₂. This suggests that the anomalously large and sample-dependent activation energy of up to 0.45 eV found in the literature¹⁸ on bulk VO₂ is related to domain structure or imperfections which are absent in the nanobeams. We find that ρ_m increases slowly with T and that at the transition $\rho_i \approx 2 \times 10^4 \rho_m$. The origin of the kink in ρ_m at 107 °C is unknown, but we note that recent experiments indicated that monoclinic distortion can occur within the metallic phase under hydrostatic pressure²⁹ or transiently after ultrafast excitation.^{7,30}

One surprise comes when we analyse the coexistence regime. Here we expect R to have four contributions:

$$R = x\rho_i^c L/A + (1-x)\rho_m^c L/A + R_c + R_{dw}, \quad (3)$$

where ρ_i^c and ρ_m^c are the insulator and metal resistivities in coexistence, and R_c and R_{dw} are the resistances of the contact to the insulator and the domain wall, respectively. Since $\rho_i \gg \rho_m$ the second term is negligible. At T_m , when the insulating domain disappears, there is usually a small, sudden drop in R of around 50 k Ω (see inset, Fig. 2a). We have yet to determine whether this reflects the resistance of the domain wall, the minimal insulating domain size, or the contact to the insulator, but in any case it implies that $R_c + R_{dw} \lesssim 50$ k Ω . Since R is usually greater than 1 M Ω for measurable x , to good accuracy we can therefore simplify Eq. (3) to

$$R = x\rho_i^c L/A. \quad (4)$$

From this relation we can determine ρ_1^c from R using values of x obtained by optical inspection. The results for a dozen nanobeams are plotted in Fig. 3 using symbols. Remarkably, to within error we see that the result is independent of T , with $\rho_1^c = 12 \pm 2 \text{ } \Omega \text{ cm}$. This means that along the phase equilibrium line the thermal activation of carriers, evident in the strong temperature dependence of ρ_1 for the unstressed insulating phase, must be perfectly compensated by the effect of changing stress given by Eq. (2). This could be a dramatic coincidence, but a much more natural explanation is that the phase transition occurs at a particular carrier density in the insulator as would be expected for a mechanism driven by electron-electron interactions. The result is therefore important new evidence that a Mott-like mechanism underlies the MIT in VO_2 .

Since ρ_1^c turns out to be constant, Eq. (4) implies that R is simply proportional to the position xL of the domain wall. We found R to be stable to within 0.1 %, limited by thermal stage stability, in a device with $L = 10 \text{ } \mu\text{m}$. This corresponds to interphase wall motion of less than 10 nm. Hence the interphase wall position, and thus the sensitivity of the transition to perturbations, may in principle be monitored with high precision by measuring R .

We turn finally to another surprising feature of the measurements with significant implications. In some nanobeams there is an additional upward step in R at some temperature below T_c that we call T_x . An example is shown in Fig. 4a, where $T_x \approx 45 \text{ } ^\circ\text{C}$. This step is always rather broad and hysteretic, often having unreproducible substructure. A clue to its origin is that the length of a buckled nanobeam increases visibly on warming across the step. Even more surprisingly, in the majority of nanobeams R jumps *upwards* when the metal domain appears at T_n (see Figs. 4b and c), rather than downwards as seen in Fig. 2. Associated with this jump there is sometimes a transient spike or short plateau in R (see insets to Fig. 4b). The behaviour is seen in both buckling and nonbuckling nanobeam sections (Fig. 4c), ruling out nonuniform strain due to buckling as a cause.

This anomalous resistance increase on warming can be explained by a transition occurring from M1 to the intermediate M2 phase, which we assume has a higher resistivity, $\rho_1^{\text{M2}} > \rho_1^{\text{M1}}$. The unit cell of M2 is longer than that of M1 along the rutile c-axis¹⁴ by a fraction $\alpha_{21} \sim 0.7\%$, causing the nanobeam to lengthen on this transition, and leading us to expect M2 to be stabilized relative to M1 by axial tension. We thus propose to include in the phase diagram a wedge-shaped region of M2, as shown in Figs. 4d to f, analogous to the M2 regions in the phase diagrams of doped^{14,15} and (110)-compressed¹⁷ VO_2 . The similar behaviour of all devices in coexistence above $68 \text{ } ^\circ\text{C}$, with the same values of ρ_1^c and dx/dT , implies that it is actually always M2 that coexists with the metal. This can explain why the value of $\alpha = 1.36 \pm 0.15 \text{ } \%$ deduced from the coexistence data is closer to the 1.6 % difference in c-axis length between M2 and metal (R) phases than to the 0.86 % difference³ between M1 and R. On the other hand, to explain the variations in behaviour between different nanobeams we find it necessary to allow the position of the M1-M2 boundary, and hence the triple-point temperature, T_{tr} , to vary. Since every device is stable in coexistence above $68 \text{ } ^\circ\text{C}$, we infer that T_{tr} is always below $68 \text{ } ^\circ\text{C}$. Lower values of T_{tr} , giving a range of temperatures where M2 is stable at $p = 0$, could be caused by differences in stoichiometry arising from different growth conditions¹⁶. The various device characteristics can now be interpreted as follows.

For a nanobeam showing no anomalous step, as in Fig. 2a, we infer that T_{tr} is below T_{room} and so the insulating phase remains M2 down to T_{room} . Indeed, the particular nanobeam of Fig. 2a exhibited an unusually large excess length ratio $\eta_0 \approx 0.9\%$ at T_{room} , which is consistent with the larger lattice constant of M2. For the case of Fig. 4a, the insulator is M1 at T_{room} , and the step

occurs at $T_x \lesssim T_{tr}$ when the nanobeam converts to M2 on reaching the M1-M2 phase boundary, as indicated in Fig. 4d. The smearing and hysteresis of the step may reflect a gradual transition via an intermediate trigonal phase, as seen¹⁴ in Cr-doped VO₂. This is indicated by the shading in Figs. 4d and f. The case of a buckled nanobeam (with small p) showing a short plateau of higher R just below T_n , as in the insets to Fig. 4b, can be interpreted as the situation where T_{tr} is just below T_c so that the temperature range over which M2 is stable is narrow (Fig. 4e).

In Fig. 3 we combine measurements from many sections of several nanobeams after excluding data for the insulating phase near T_x where the behaviour is hysteretic. The insulator resistivity then falls onto two curves: the upper we identify with ρ_i^{M2} , and the lower with ρ_i^{M1} . We find that the ratio $\rho_i^{M2}/\rho_i^{M1} = 3.0 \pm 0.1$ is independent of T , implying that M1 and M2 have same energy gap.

One point deserves emphasis: we never see the metallic phase appear directly from the M1 phase, which would produce a drop in resistance from the fully M1 level. Either we see a step up in resistance as in Figs. 4b and c, signifying a direct M1 \rightarrow (M2+metal) transition, or we see an intermediate and often transient M2 state, ie, M1 \rightarrow M2 \rightarrow (M2+metal), as in Fig. 4a and the insets to Fig. 4b. This is true even in unbuckled nanobeams (Fig. 4c) where positive pressure should mean that the M1-metal phase boundary is reached first on warming, as indicated in Fig. 4f. We conclude that on warming the VO₂ remains in the M1 phase until some M2 phase appears. In many cases M1 has already become unstable with respect to the metal by that point, as indicated in Fig. 4f, and as soon as M2 appears the nanobeam quickly relaxes to its thermodynamically stable (M2+metal) coexistence state which has a larger total resistance.

The above finding, that the insulator-metal transition occurs not directly from the M1 phase but rather only from the intermediate M2 phase, combined with our conclusion that it happens at a particular carrier density in the M2 phase, suggests that the MIT involves a Mott-like transition occurring in the undimerized vanadium chains present only in the M2 phase. The need to unpair these chains could explain the 75 fs timescale of the transition driven optically from the M1 phase,⁸ and suggests that the transition from M2 may be faster. In conclusion, our results show that there are many advantages to be gained from working with strongly correlated materials in nanoscale crystalline form.

References

- ¹ Morin, F.J., Oxides which show a metal-to-insulator transition at the Neel temperature. *Physical Review Letters* **3** (1), 34 (1959).
- ² Mott, N.F., *Metal-Insulator Transitions*, 2nd ed. (CRC, 1990).
- ³ Eyert, V., The metal-insulator transitions of VO₂: a band theoretical approach. *Ann. Phys.* **11** (9), 53 (2002).
- ⁴ Verleur, H.W., Barker, A.S., and Berglund, C.N., Optical properties of VO₂ between 0.25 and 5 eV. *Physical Review* **172** (3), 788 (1968).
- ⁵ Becker, M.F., Buckman, A.B., and Walser, R.M., Femtosecond laser excitation of the semiconductor-metal phase transition in VO₂. *Applied Physics Letters* **65** (12), 3 (1994).
- ⁶ Petrov, G.I., Yakovlev, V.V., and Squier, J.A., Nonlinear optical microscopy analysis of ultrafast phase transformation in vanadium dioxide. *Optics Letters* **27** (8), 3 (2002).
- ⁷ Kim, H.-T. et al., Monoclinic and correlated metal phase in VO₂ as evidence of the Mott transition: coherent phonon analysis. *Physical Review Letters* **97**, 4 (2006).

- 8 Cavalleri, A., Rini, M., and Schoenlein, R.W., Ultra-broadband femtosecond
measurements of the photo-induced phase transition in VO₂: from the mid-IR to the hard
9 X-rays. *J. Phys. Soc. Japan* **75** (1), 9 (2006).
- 10 Hilton, D.J. et al., Enhanced photosusceptibility near T_c for the light-induced insulator-to-
metal phase transition in vanadium dioxide. *Physical Review Letters* **99** (22) (2007).
- 11 Baum, P., Yang, D.-S., and Zewail, A.H., 4D Visualization of Transitional Structures in
Phase Transformations by Electron Diffraction. *Science* **318**, 788 (2007).
- 12 Kubler, C. et al., Coherent structural dynamics and electronic correlations during an
ultrafast insulator-to-metal phase transition in VO₂. *Physical Review Letters* **99** (11)
(2007).
- 13 Umeda, J.-i., Ashida, S., Kusumoto, H., and Narita, K., A new phase appearing in metal-
semiconductor transition in VO₂. *J. Phys. Soc. Japan* **21**, 1461 (1966).
- 14 Zylbersztejn, A. and Mott, N.F., Metal-insulator transition in vanadium dioxide. *Physical
Review B* **11** (11), 4383 (1975).
- 15 Marezio, M., McWhan, D.B., Remeika, J.P., and Dernier, P.D., Structural aspects of the
metal-insulator transitions in Cr-doped VO₂. *Physical Review B* **5** (7), 2541 (1972).
- 16 Pouget, J.P. et al., Dimerization of a linear Heisenberg chain in the insulating phases of
V_{1-x}Cr_xO₂. *Physical Review B* **10** (5), 1801 (1974).
- 17 Chamberland, B.L., New defect vanadium dioxide phases. *Journal of Solid State
Chemistry* **7**, 377 (1973).
- 18 Pouget, J.P., Launois, H., D'Haenens, J.P., Merenda, P., and Rice, T.M., Electron
localization induced by uniaxial stress in pure VO₂. *Physical Review Letters* **35** (13), 873
(1975).
- 19 Berglund, C.N. and Guggenheim, H.J., Electronic properties of VO₂ near the
semiconductor-metal transition. *Physical Review* **185** (3), 1022 (1969).
- 20 Allen, P.B., Wentzcovitch, R.M., Schulz, W.W., and Canfield, P.C., Resistivity of the
high-temperature metallic phase of VO₂. *Physical Review B* **48** (7), 4359 (1993).
- 21 Qazilbash, M.M. et al., Correlated metallic state of vanadium dioxide. *Physical Review B*
74 (20) (2006).
- 22 Wentzcovitch, R.M., Schulz, W.W., and Allen, P.B., VO₂: Peierls or Mott-Hubbard? A
view from band theory. *Physical Review Letters* **72** (21), 3389 (1994).
- 23 Rice, T.M., Launois, H., and Pouget, J.P., Comment on "VO₂: Peierls or Mott-Hubbard?
A View from Band Theory". *Physical Review Letters* **73** (22), 3042 (1994).
- 24 Qazilbash, M.M. et al., Mott Transition in VO₂ Revealed by Infrared Spectroscopy and
Nano-Imaging. *Science* **318**, 1750 (2007).
- 25 Guiton, B.S., Gu, Q., LPrieto, A., Gudiksen, M.S., and Park, H., Single-Crystalline
Vanadium Dioxide Nanowires with Rectangular Cross Sections. *Journal of the American
Chemical Society* **127**, 2 (2005).
- 26 Wu, J. et al., Strain-induced self organization of metal-insulator comains in single-
crystalline VO₂ nanobeams. *Nano Letters* **6** (10), 5 (2006).
- 27 Tsai, K.Y., Chin, T.S., and Shieh, H.P.D., Effect of grain curvature on nano-indentation
measurements of thin films. *Japanese Journal of Applied Physics Part 1* **43** (9A), 6268
(2004).
- Minomura, S. and Nagasaki, H., The effect of pressure on the metal-to-insulator
transition in V₂O₄ and V₂O₃. *Journal of the Physical Society of Japan* **19**, 131 (1964).

- 28 Kucharczyk, D. and Niklewski, T., Accurate X-ray determination of the lattice
parameters and the thermal expansion coefficients of VO₂ near the transition temperature.
Journal of Applied Crystallography **12** (4), 4 (1979).
- 29 Arcangeletti, E. et al., Evidence of a pressure-Induced metallization process in
monoclinic VO₂. *Physical Review Letters* **98**, 4 (2007).
- 30 Rosevear, W.H. and Paul, W., Hall-effect in VO₂ near the semiconductor-to-metal
transition. *Physical Review B* **7** (5), 2109 (1973).

Acknowledgments

We thank Anton Andreev, Boris Spivak, Oscar Vilches and Younan Xia for discussions, Volker Eyert and Hyun-tak Kim for comments on the manuscript, and Jacob Beedle, Megan Campbell and Conor Sayres for experimental assistance. This work was supported by the Army Research Office under contract number 48385-PH, and employed facilities in the UW Nanotech Center. WC and ZW were partially supported by UW UIF Nanotech fellowships.

Author contributions

JW performed the experiments with assistance from ZW and WC. DHC mainly provided guidance and analysis and wrote the manuscript.

Author information

Correspondence and requests for materials should be addressed to cobden@u.washington.edu.

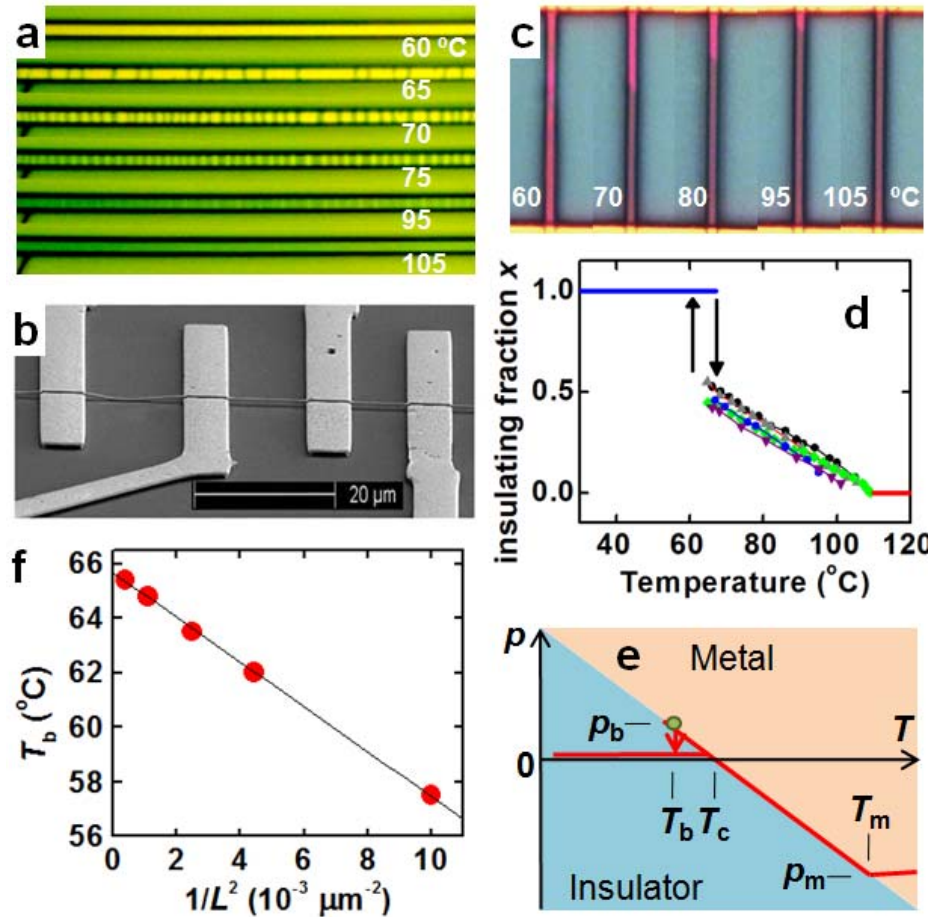


Figure 1 Metal-insulator transition in VO_2 nanobeams studied by microscopy. **a**, Six images of a $40\ \mu\text{m}$ -long part of a single nanobeam attached as grown to an SiO_2 substrate, taken at the indicated temperatures during warming, showing metallic domains (darker) appearing, widening and merging. **b**, SEM image of a suspended nanobeam device showing that longer sections are buckled at room temperature. **c**, Five images of one suspended nanobeam between contacts at the top and bottom separated by $20\ \mu\text{m}$. Above $68\ ^\circ\text{C}$ it contains a single metallic domain (grey), which grows on warming until the insulating domain (purple) disappears at about $105\ ^\circ\text{C}$. **d**, Plot of the insulating fraction x vs. T for six suspended nanobeams of various dimensions. **e**, Sketch of the phase diagram indicating part of the trajectory (red) followed on a temperature cycle. The vertical axis is uniaxial pressure p . The green circle indicates the point at which the nanobeam buckles on cooling. **f**, Plot of buckling temperature T_b vs. inverse square length for a nanobeam (thickness $H = 0.18\ \mu\text{m}$, width $W = 0.9\ \mu\text{m}$) yields a straight line whose y -intercept should be T_c .

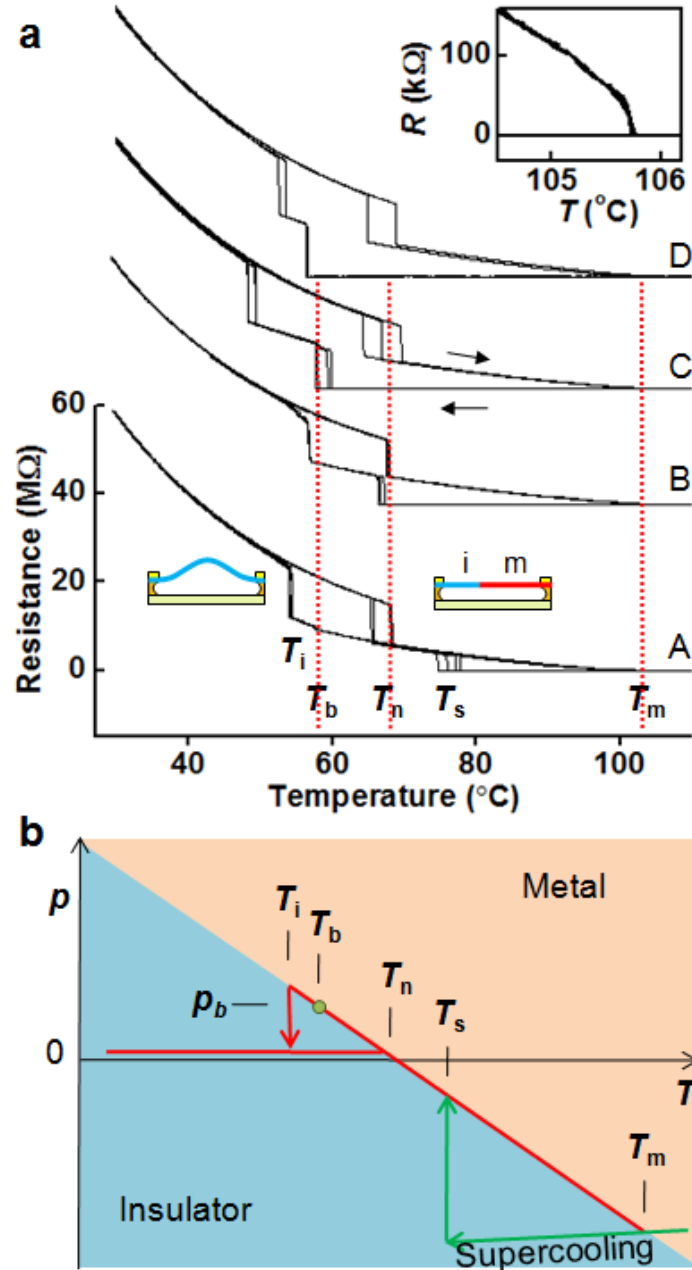


Figure 2 a, Characteristics of four sections, designated A-D, of one nanobeam, each having $L = 26$, $H = 0.25$, and $W = 0.7 \mu\text{m}$. Each section is buckled and fully insulating at $30 \text{ }^\circ\text{C}$ (left inset sketch), and straight and coexisting at $90 \text{ }^\circ\text{C}$ (right inset sketch). Inset: a repeatable small jump of about $50 \text{ k}\Omega$ is seen as the insulator disappears near T_m . **b**, Corresponding phase diagram. The red line indicates the trajectory followed by section A. On warming the nanobeam unbuckles and jumps from fully insulating to coexistence at T_n , and becomes fully metallic at T_m . On cooling it supercools to T_s at which the insulator nucleates, it buckles downwards at T_b , and it then buckles upwards and becomes fully insulating at T_i .

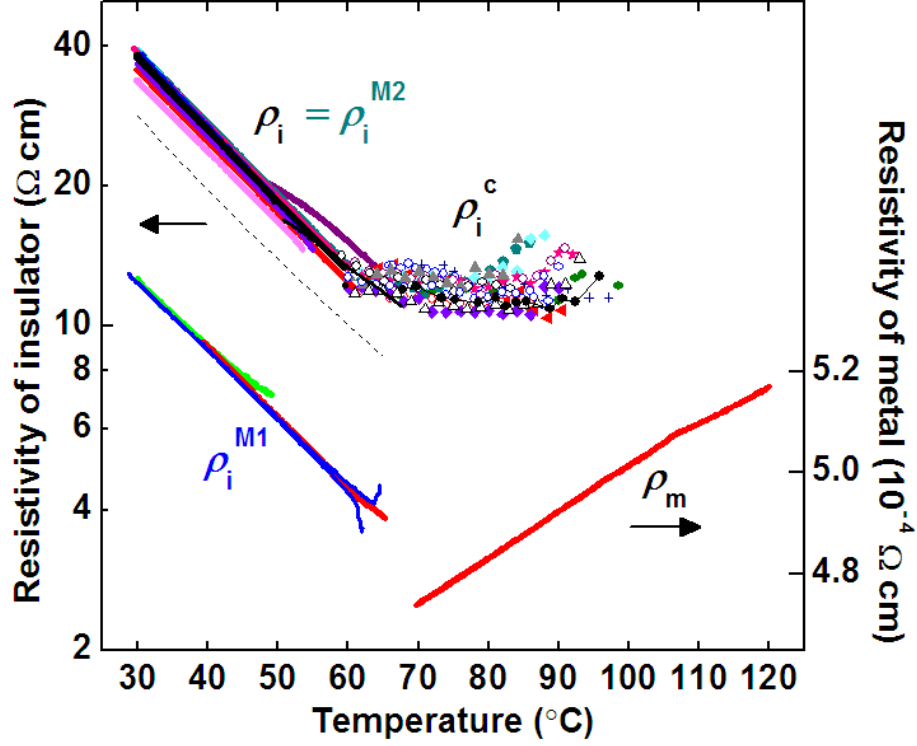


Figure 3 Collected resistivity measurements for twelve nanobeams of various dimensions. The insulator resistivity ρ_i follows two distinct curves, which we ascribe to the M1 and M2 phases, both of which exhibit an activation energy of 0.30 eV (illustrated by the dotted line). Plotted using symbols are measurements of the resistivity ρ_i^c of the insulator in coexistence for ten different nanobeams. To within error they show a universal temperature-independent value of $12 \pm 2 \Omega\text{cm}$. The metal resistivity ρ_m was obtained from one section of a nanobeam ($H = 0.18$, $W = 0.9$, $L = 30 \mu\text{m}$) from which two other different-length sections ($L = 20$ and $50 \mu\text{m}$) gave almost identical results. We estimate the error in ρ_m due to uncertainty in the cross-section to be 25%.

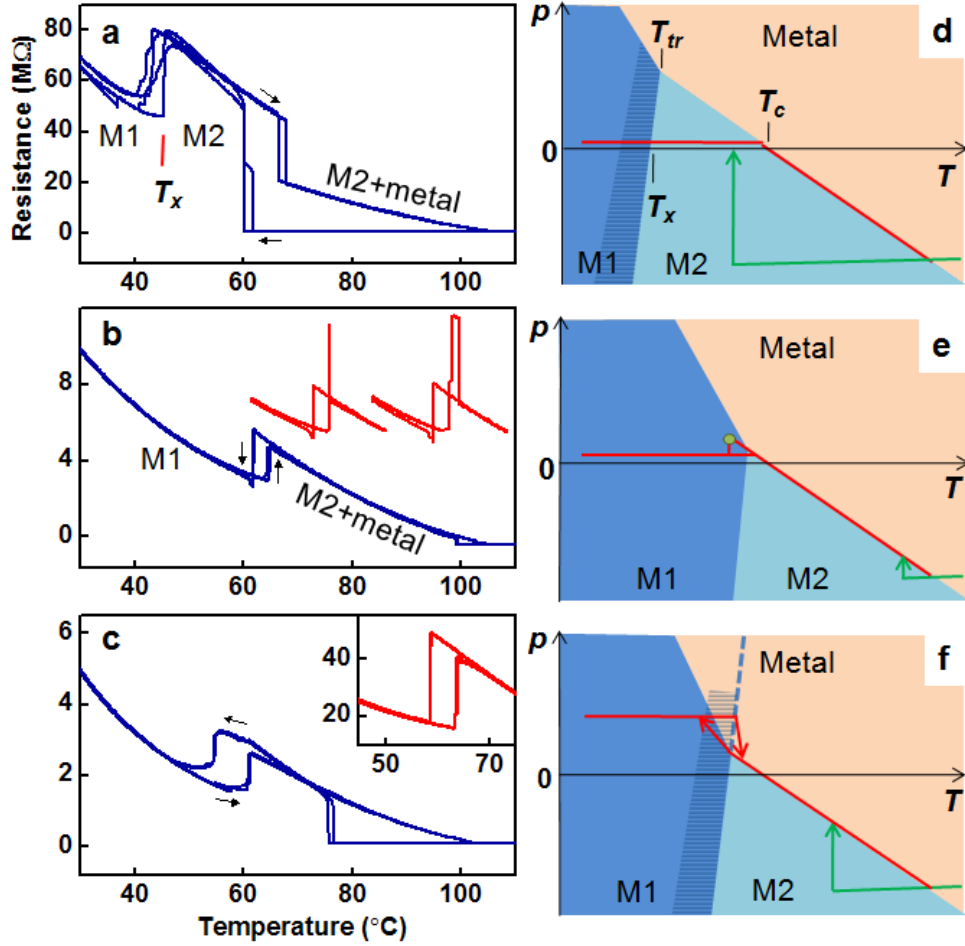


Figure 4 Anomalous behaviour of R vs T and its interpretation on phase diagrams incorporating both M1 and M2 insulating phases. **a**, Repeated temperature cycling of a buckling nanobeam ($L = 20$, $H = 0.12$, $W = 0.5 \mu\text{m}$) showing an additional resistance jump at T_x . This is explained by crossing the M1-M2 phase boundary with a relatively low triple-point temperature T_{tr} , as indicated in diagram **d**. **b**, Buckling nanobeam ($L = 13$, $H = 0.12$, $W = 1.0 \mu\text{m}$) where R jumps up as the metal appears, sometimes with an intermediate transient spike (insets), explained by T_{tr} being close to T_c as in diagram **e**. **c** Unbuckling nanobeam ($L = 1.4$, $H = 0.23$, $W = 0.56 \mu\text{m}$) showing similar behaviour, implying the M1-metal transition occurs not directly but only via M2, as indicated in diagram **f**. Inset: another example from a buckled nanobeam. Shading in phase diagrams **d-f** indicates region of apparent gradual nature of the M1-M2 transition observed when T_{tr} is not close to T_c . Supercooling is again shown in green.